Electron self-injection during interaction of tightly focused few-cycle laser pulses with underdense plasma

Alexei Zhidkov, Takashi Fujii, and Koshichi Nemoto
Central Research Institute of Electric Power Industry, 2-6-1 Nagasaka, Yokosuka-shi, Kanagawa-Ken, 240-0196, Japan
(Received 9 April 2008; revised manuscript received 11 July 2008; published 19 September 2008)

We study the interaction of short laser pulses tightly focused in a tiny volume proportional to the cube of the pulse wavelength (λ^3) with underdense plasma by means of real-geometry particle-in-cell simulations. Underdense plasma irradiated by relatively low-energy λ^3 (and λ^2) laser pulses is shown to be an efficient source of multi-MeV electrons, ~50 nC/J, and coherent hard x rays, despite a strong pulse diffraction. Transverse wave breaking in the vicinity of the laser focus is found to give rise to an immense electron charge loading to the acceleration phase of a laser wake field. A strong blowout regime provoked by the injected electrons resulting in the distribution of accelerated electrons is found for λ^3 pulses (further electron acceleration driving by λ^2 pulses runs in the usual way). With an increase of pulse energy, wiggling and electron-hose instabilities in the λ^3 pulse wake are recognized in the blowout regime. For higher-energy λ^3 pulses, the injected beams are well modulated and may serve as a good source of coherent x rays.

DOI: 10.1103/PhysRevE.78.036406 PACS number(s): 52.38.Kd, 41.75.Jv, 52.38.Hb

I. INTRODUCTION

Recent progress in laser-plasma electron acceleration [laser wake field acceleration (LWFA)]—the generation of 1-GeV monoenergetic electron beams, tens of MeV, low-emittance electrons with their total charge over 1 nC and high beam stability, and others [1,2]—has raised interest to this new class of compact accelerators and x-ray radiation sources based on very dense electron beams. The use of a laser system with a low pulse energy ε and a high repetition rate for those purposes is very attractive: a laser pulse focused in a plasma with its waist $w_0 \sim \lambda$, where λ is the laser wavelength, and with its duration τ of a few cycles (λ^3 pulse) reaches the relativistic intensity and generates relativistic plasma at a relatively low pulse energy [3–5]; a high repetition rate of low-energy laser systems could provide a practically high fluence of energetic electrons and x rays. Poor pulse self-guiding and different electron self-injection in the acceleration phase of laser wake make the λ^3-interaction regime distinct from the known "bubble" regime [1]. Even though presently few-cycle laser pulses reach only a few mJ and are far from the requirements of laser particle acceleration, a comprehensive study of the interaction of tightly focused laser pulses with underdense plasma including the effects of propagation, wake field generation, and electron acceleration may become a good boost for further development of the λ^3-laser technique.

LWFA can be conditionally subdivided into two parts: electron injection and electron acceleration. Electron injection is a key part of the whole process responsible for the total charge, emittance, and energy spread of accelerated electrons [1,2,6–11]. In one-pulse-acceleration schemes, the electron injection is the self-injection and, usually, is a result of plasma wave breaking [6] provoked by plasma nonuniformity.

The value of a self-injected charge is very sensitive to the laser parameters: it exponentially increases with the laser intensity in the vicinity of injection [2,10]. Therefore in the case of a tightly focused, few-cycle laser pulse, an increase of total charge with intensity can overcome a charge decrease due to a smaller laser waist, and the pulse, therefore, could generate a beam with a charge much higher than that generated by a conventional pulse with the same energy. The electron acceleration stage does not change much with the laser intensity; however, the pulse intensity is required to be constant during pulse propagation over the dephasing length [12] until an injected electron acquires the maximal energy. This needs a good self-guiding that should be achieved at $P=\varepsilon/\tau > P_{\mathrm{cr}}=1.7\times 10^{-2} N_{\mathrm{cr}}/N_e$ TW (P and P_{cr} are the pulse power and the critical power; N_e and N_{cr} are the electron density and the critical density) and seems to become softer for a shorter laser pulse.

However, such a direct scaling of the results of high-power laser pulse experiments [1–11] to the interaction of λ^2 and λ^3 laser pulses with underdense plasma is hardly correct: diffraction exerts a much stronger influence on the laser-plasma interaction in the case of tightly focused laser pulses. An efficient length of a tightly focused laser pulse L is of the order of the pulse Rayleigh length; the ratio $L/\lambda_p \sim L_R/\lambda_p = \pi(w_0/\lambda)^2(N_e/\gamma N_{\mathrm{cr}})^{1/2} \sim \pi(N_e/a_0 N_{\mathrm{cr}})^{1/2}$ (λ_p is the plasma wavelength and $\gamma \sim a_0$ is the electron relativistic factor in the external laser field with amplitude $a_0 \gg 1$) becomes less than 1 in underdense plasma. For λ^3 laser pulses this ratio is always less than 1. As has been shown in Ref. [12] for such laser pulses, the self-guiding may not appear in uniform or weakly nonuniform plasma even for a laser pulse with its power exceeding the critical power. The use of plasma channels for pulse guiding may strongly result in the dynamics of the laser-plasma interaction. Therefore, a theoretical study of the propagation of tightly focused laser pulses can be done only in the real geometry because the laser intensity is proportional to w^2.

Due to the shorter Rayleigh length, the focus position of tightly focused pulses is also a key parameter of the laser-plasma interaction. It is apparent that the maximal intensity is reached if a λ^3 pulse is focused in the plasma bulk; there, it becomes practically impossible to use a steep density gradient to boost the longitudinal wave breaking [10] for the

electron self-injection. Fortunately, if laser pulses are tightly focused down to $w_0 \sim \lambda$, they cannot leave behind even a half-period of the regular wake [6,11]; the strong transverse wave breaking limited by the pulse diffraction may be an efficient mechanism of electron self-injection.

In the present paper, we report results of fully relativistic particle-in-cell simulations of the interaction of λ^3 laser pulses ($\lambda=0.8$ μm) with underdense plasma in the real geometry. The three-dimensional (3D) particle-in-cell (PIC) FPLASER3D code [9,11] employing square weighting for currents and the "moving window" technique (in the figures the laser pulse propagates from the right to left) is used. The initial conditions for the transverse components of the fields are taken as the well-known solution of the parabolic equation [13,14]

$$E_z(x-x_f,r) = -B_y(x-x_f,r) = A_0[w_0/w(x-x_f)]\exp(-r^2/w^2(x - x_f) - 2x^2/(c\tau)^2 + ikx + i\phi(x-x_f,r)\ ,$$

where x_f is the focus position, $w(x-x_f)$ is the beam waist, $w_0=1.5$ μm, and ϕ is the phase. The longitudinal components are found from the equations $\vec{\nabla}\cdot\vec{E}=0$ and $\vec{\nabla}\cdot\vec{B}=0$. No time-dependence correction [14] has been included in the initial conditions. However, the number of calculation steps is enough to adjust the field strength to a solution of Maxwell's equation before the pulse is focused in the plasma. We use nine particles per cell $[\Delta X\times\Delta Y\times\Delta Z=(\lambda/15)\times(\lambda/9)^2]$ in a (80 μm)$\times$(40 μm)^2 window that moves at the speed of light. Linearly (in the z axis) polarized full width at half maximum (FWHM) laser pulses with their energy 15 mJ, 150 mJ, and 1 J [15] have duration $\tau=8$ fs and 32 fs. Initially the laser pulse is set at $x_0-x_f=60$ μm far from its focus point $x_f=20$ μm behind the laser-vacuum interface. The plasma electron density ranges from $N_e=10^{19}$ to $N_e=10^{20}$ cm^{-3}. At the plasma-vacuum interface, the plasma density linearly decreases to zero in 10 μm. The plasma density is uniform transversely or has a parabolic shape emulating a plasma channel of 80 μm diameter and with minimal density equal to 1/3 or 1/8 of the maximal. Such narrow and high-density plasma channels have been generated recently with the use of picosecond prepulses copropagating with the main pulse in a gas jet in an external magnetic field [16].

II. LOW-ENERGY LASER PULSES

In the beginning we make PIC runs for low-energy λ^3 and λ^2 laser pulses, $\varepsilon=15$ mJ in uniform plasma and plasma channels. At fixed pulse energy, the power of the pulses depends on the pulse duration: for the λ^2 pulses it is equal to $P=0.5$ TW and for the λ^3 pulses $P=2$ TW. With focus spot $w_0=1.5$ μm, it gives $a_{0\max}=2.46$ and $a_{0\max}=4.9$, respectively. The self-guiding requires the plasma density $N_e>6\times10^{19}$ cm^{-3} and $N_e=1.5\times10^{19}$ cm^{-3} for the pulses, respectively. However, numerically we observe no self-guiding of λ^3 laser pulses in uniform plasma even for a density that much exceeds the critical density.

In Figs. 1 and 2, the evolution of laser pulses is shown for different plasma densities $N_e=3\times10^{19}$ cm^{-3} and $N_e=2\times10^{20}$ cm^{-3}. In the case of lower density, we observe diffraction almost as strong as the diffraction in vacuum even though the pulse power exceeds the critical power. Plasma effects appear as a stronger focusability of the pulse, $a_0=5.7$, in the vicinity of the focus position versus $a_0=4.9$ in vacuum, and slower diffraction, $E/E_{\text{vacuum}}(x=10L_R)=2.7$. According to the 1D approximation given in Ref. [17], the critical power for a pulse with its length L shorter than the plasma wavelength λ_p increases by a factor of $(2/\pi^2)(\lambda_p/L)^2$. For this particular case, the factor equals 1.28, while the density exceeds the critical density by a factor of 2. We attribute this difference to a stronger diffraction in the real geometry.

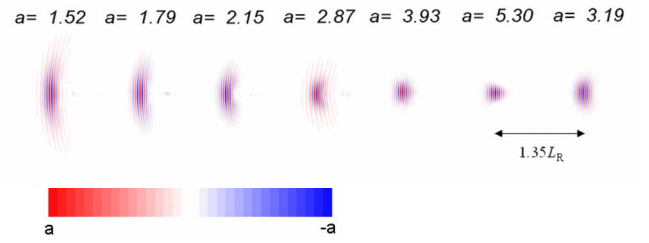

FIG. 1. (Color online) Dynamics of the z component of the electric field of a 15-mJ λ^3 pulse focused in a uniform plasma with $N_{e0}=3\times10^{19}$ cm^{-3}. The laser pulse propagates from the right to left; the distance of output and the maximal value of the field, a, are given in the figures.

With the density increase, we find a rapid decrease of the laser field with its propagation into plasma bulk. However, this is the result of strong stimulated Raman scattering (SRS) with the formation of solitonlike waves [18] in the laser wake (see Fig. 2). Figure 3, showing the longitudinal plasma field (a) and plasma density (b), (c) in the pulse wake, also illustrates the formation of solitonlike electromagnetic waves: electromagnetic solitons with velocity considerably less than the speed of light and a typical density modulation are marked by asterisks. (A comprehemsive discussion of the process of soliton formation is given in Ref. [18] and in references therein.) As a result, the λ^3 pulse becomes longer (see Fig. 2) with corresponding decreases in its intensity. Therefore, a simple increase of plasma density is not enough to provide the λ^3 pulse self-guiding.

At first sight, there must be no accelerated electrons. The pulse is too weak in the vicinity of the plasma-vacuum interface to provoke a considerable wave breaking. However,

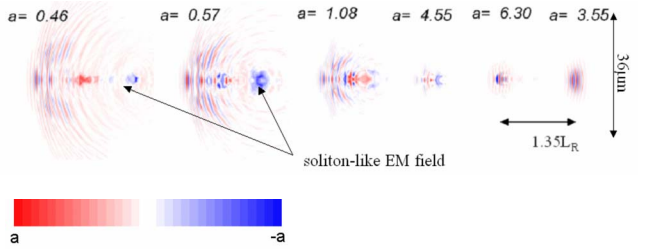

FIG. 2. (Color online) Dynamics of the z component of the electric field of a 15-mJ λ^3 pulse focused in a uniform plasma with $N_{e0}=3\times10^{20}$ cm^{-3}. The laser pulse propagates from the right to left; the distance of output and the maximal value of the field, a, are given in the figures.

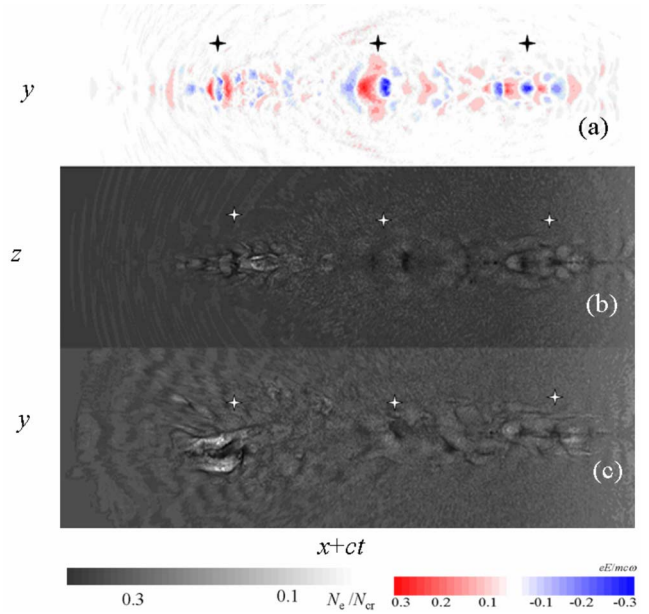

FIG. 3. (Color online) Spatial distribution of the plasma field, E_x (a), and electron density, N_e (b),(c), in the plane crossing the laser axis (a),(b) perpendicular and (c) parallel to the pulse polarization at $N_{e0}=3\times10^{20}$ cm^{-3} at distance $x=8.1L_R$ from the focus position. Asterisks show the positions of electromagnetic solitons.

strong transverse wave breaking appears in the vicinity of the focus position where the laser waist is minimal; according to Ref. [19], there must be no intact period behind the tightly focus laser pulse. We observe this numerically: the self-injection of plasma electrons in the acceleration phase of the laser pulse wake appears in the vicinity of the focus point. This is detected as a position where electrons with energy enough for injection appear first. There is no essential injection in the vicinity of the longitudinal density gradient (the pulse intensity is too low yet and a loaded charge is far much less than that loaded in the focus) and no further continuous injection, resulting in an increase of the charge of the accelerated electrons (the pulse intensity is too low after diffraction). The electron self-injection is shown Fig. 4. One can see that this is a collective process accompanying the wave breaking; the wave structure of the injection is clearly seen in Fig. 4(c) with the transverse distribution of injected electrons. As the result of this self-injection, the electrons are accelerated by the laser wake. Their energy distributions are shown in Fig. 5; it is a Maxwell-like distribution with an efficient temperature. In spite of a very short acceleration length the maximal energy of electrons achieves 40 MeV in the case of low-density plasma; the total charge of accelerated electrons with energy over 5 MeV exceeds 1.2 nC. In higher-density plasma the electron maximal energy is expectedly smaller, 12 MeV. However, the charge of electrons with the energy over 5 MeV is about 2.1 nC. Such electrons may be an efficient source of hard, over 1 MeV, x rays.

The next runs are performed for plasma channels. (As shown in Ref. [20], such channels can be drilled in a plasma by laser prepulses in the presence of a magnetic field.) The propagation of λ^3 laser pulses is supposed to be dramatically different in this case [18]. In the paraxial approximation the

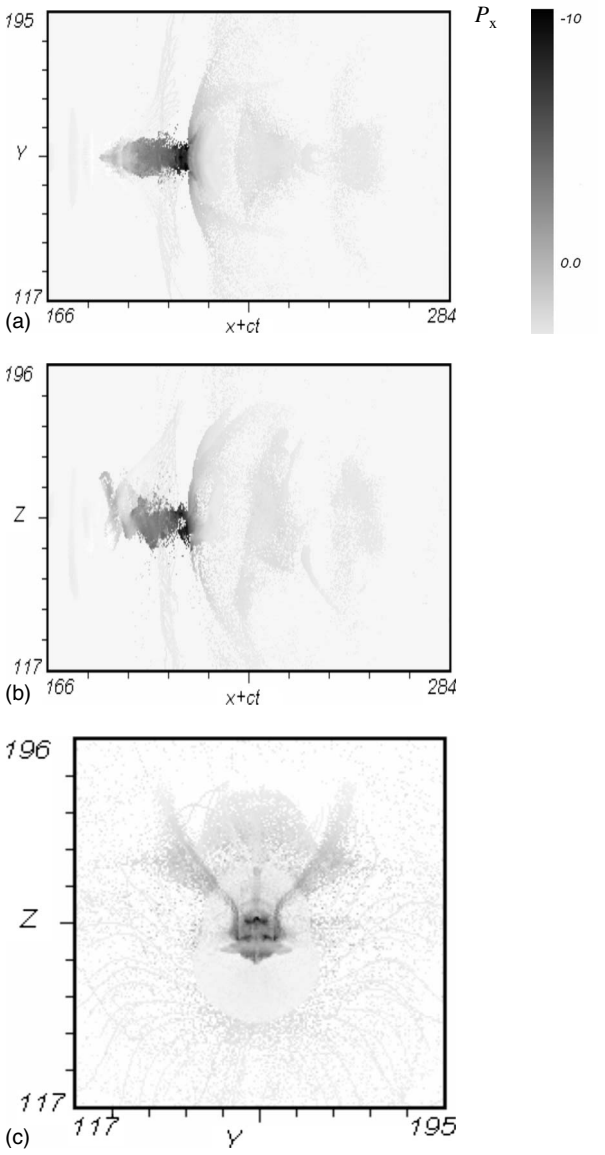

FIG. 4. Spatial distribution of the x component of the momentum of an electron self-injected in the vicinity of the laser focus: (a) the plane $z=0$, (b) the plane $y=0$, and (c) $x+ct=200$.

waist of a laser pulse in a plasma channel with the transverse density profile as $N_e(r)=N_e(0)[1+\Delta(r/D)^2]$ obeys the equation [12,20,21]

$$\frac{d^2R}{dX^2}\approx\frac{\lambda}{4\pi L_R R^3}\left[1-\frac{4\pi L_R}{\lambda\bar{\gamma}}\frac{N_{eD}}{N_{\rm cr}}\left(\frac{w_0}{D}\right)^2R^4\right],\qquad(1)$$

where $\bar{\gamma}\approx\sqrt{1+a_0^2/2}$ is an effective relativistic factor of plasma electrons; R is the pulse waist normalized on the minimal waist w_0; $X=x/w_0$, x is the coordinate in the direction of laser pulse propagation; $N_{eD}=N_e(0)\Delta$. According to Eq. (1), the condition of the pulse guiding does not depend on the channel depth and the minimal laser pulse waist. The near-equilibrium waist of a laser pulse is approximately $w\approx(D\lambda)^{1/2}[N_{\rm cr}\bar{\gamma}/4\pi^2N_{eD}]^{1/4}$. For $N_{eD}=N_{\rm cr}$, $D=10\lambda$, and $\bar{\gamma}=4$ one can estimate $w=1.8\lambda$, which exceeds the laser wavelength. It is difficult to confine a relativistically intense and

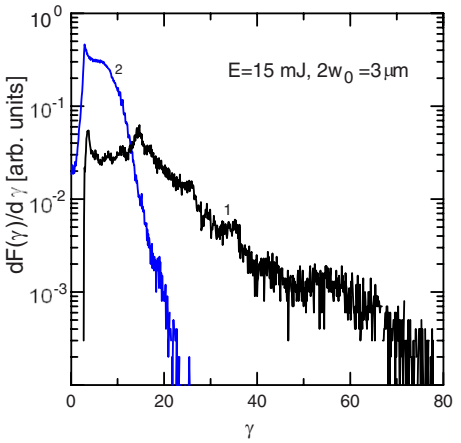

FIG. 5. (Color online) Energy distribution ($\gamma=\varepsilon/mc^2$) of electrons accelerated by 15-mJ λ^3 laser pulses in low-density (1) and higher-density (2) plasma.

tightly focused laser pulse with $w_0 \approx \lambda$ in an underdense plasma channel. However, the use of a plasma channel may allow much longer electron acceleration in the laser wake.

The evolution of 15-mJ λ^3 laser pulses in a shallow channel, $\Delta=3$, is shown in Fig. 6 and $N_{eD}=6\times10^{19}$ cm^{-3}. In the beginning, the pulse diffracts very similarly to the case of uniform plasma as presented in Fig. 1. Then one can see a long guiding of the pulse at a moderate intensity $a_0 \sim 1$ with its waist much exceeding the minimal. The forward SRS of the pulse results in a pulse elongation. After the pulse exceeded approximately 160 μm, its length became 8 times as long as the initial length; the corresponding frequency downshift is clearly seen. The radiation field of accelerated electrons is also seen behind the laser pulse.

Electron self-injection appears again in the vicinity of the focus position. The dynamics of the self-injected electrons is shown in Fig. 7. The injection time is very short, and therefore the electrons are injected only in the first bucket of the laser wake. (Even though a well-structured plasma field arises in the pulse wake [see Fig. 7(c)], there is no further essential injection and electron acceleration.) Strong electron blowout is displayed in the first bucket. Initially, this is a result of the ponderomotive evacuation of plasma electrons by the tightly focused laser field. Later, the blowout is the result of the expulsion of plasma electrons by the electron beam. In the beam, the electrons constitute a modulated

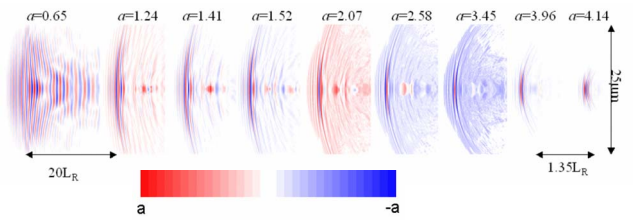

FIG. 6. (Color online) Dynamics of the z component of the electric field of a 15-mJ λ^3 pulse focused in a plasma with $N_{eD}=6\times10^{19}$ cm^{-3} and $\Delta=3$. The laser pulse propagates from the right to left; the distance of output and the maximal value of the field, a, are given in the figures.

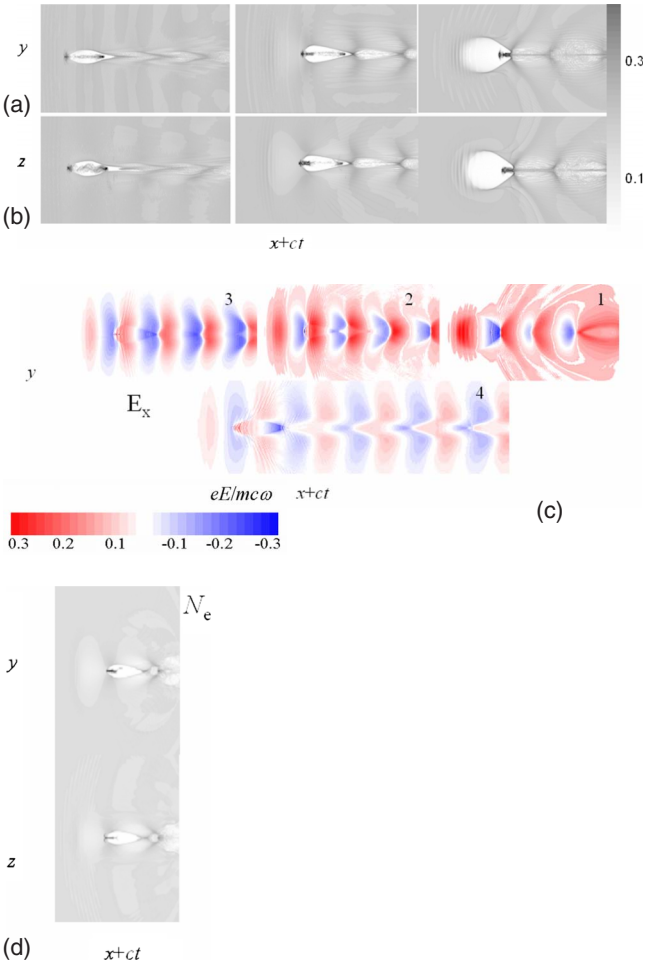

FIG. 7. (Color online) Dynamics of the electron density and x component of the plasma field in plasma channels irradiated by a 15-mJ λ^3 pulse. $N_{eD}=6\times10^{19}$ cm^{-3}; (a), (b), (c) $\Delta=3$ and (d) $\Delta=8$. In (a), (b), and (c) snapshots done after a propagation distance equal to $5L_R$ and (d) the distance equals $8L_R$ from the focus position. The numbers in (d) are given for easier recognition of the snapshots. The pulse propagates from the right to left.

beam with a total charge of about 0.7 nC. Such a charge is large enough to produce the electron blowout which is relative to that in the plasma wake field acceleration [22]. A run performed for a deeper channel, $\Delta=8$, gives very similar results [see Fig. 7(d)], as should follow from Eq. (1). However, the electron energy distribution is different. The energy distributions for both $\Delta=3$ and $\Delta=8$ are given in Fig. 8. In the case of the deeper channel this distribution consists of several quite monoenergetic peaks, while the shallower channel gives a broad distribution in the higher-energy range. This reflects the effects of charge loading discussed in Ref. [11]: this broader distribution is a result of stronger electron thermalization in the higher-density plasma. Multiple peaks in the electron energy distribution in the deeper channel appear as a result of multiple self-injections similar to that shown in Ref. [11]. With a much deeper channel, a single monoenergetic bunch with a low charge could be generated. However, the strong diffraction of λ^3 laser pulses limits the energy of the electrons to below a few MeV. In the case of the λ^2 laser pulse, the single monoenergetic bunch limit may

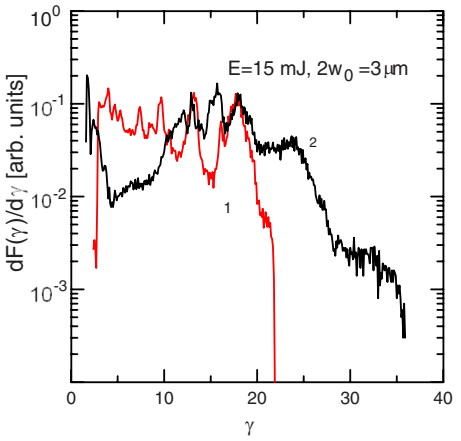

FIG. 8. (Color online) Energy distribution of electrons accelerated by 15-mJ λ^3 laser pulses in the plasma channels $\Delta=8$ (1) and $\Delta=3$ (2).

be achieved with a higher energy of accelerated electrons.

An increase of N_{eD} up to 3×10^{20} cm^{-3} at $\Delta=3$ results in a considerable increase of the total charge of accelerated electrons. Moreover, in such a higher-density channel, the guiding of the λ^2 laser pulse with much lower intensity becomes possible. The plasma density distribution after the λ^2 and λ^3 laser pulses pass the vicinity of the focus is shown in Fig. 9 in the plane perpendicular to the pulse polarization [(a), (c)] and in the transverse plane [(b), (d)]. In the case of the λ^2 laser pulse there is also no regular plasma wave in the vicinity of the focus (shown by circle 1); the density ripple is quite stochastic. However, after the laser pulse passed the distance exceeding the Rayleigh length and slightly diffracted, the common wake arises (marked by circle 2 in Fig. 9). Only electrons with small transverse momentum are injected. As seen in Fig. 9(b), the beam has an asymmetric shape; its diameter is of the order of $2w_0$. The total charge of the injected electrons is about 60 pC. The injected electrons do not change the structure of the plasma wave notably; therefore, the λ^2 interaction has a scenario typical of the LWFA with a quite efficient self-injection. In the case of a λ^3 laser pulse, the injection is more efficient; the injected charge is immense, about 1.2 nC, with a strong effect on the laser wake. The difference, the order of magnitude, in the injected charge is the result of an increase of the laser intensity. In Figs. 9(c) and 9(d) one can see a cavity in the electron density distribution. The cavity is the result of the evacuation of the injected electrons by their electrostatic field. In contrast to the conventional blowout regime in the PWFA, the electrons on the cavity surface in this case are also the self-injected relativistic electrons. Assuming a spherical distribution of the injected electrons, one may find the energy of the interaction of an electron with the bunch: $W\sim e^2N/2R$, where N is the number of electrons in the bunch and R is radius of the sphere. For a 1-nC injection and $R\sim3$ μm, it gives $W=1.5$ MeV, which is comparable to the energy of accelerated electrons. This explains the appearance of effects of charge loading. The density distribution in the cavity is shown in Fig. 10. An image of the cavity is given in Fig. 10(a). The 1D projections of the electron density are given in Figs. 10(b) and 10(c) for a better numerical analysis of the

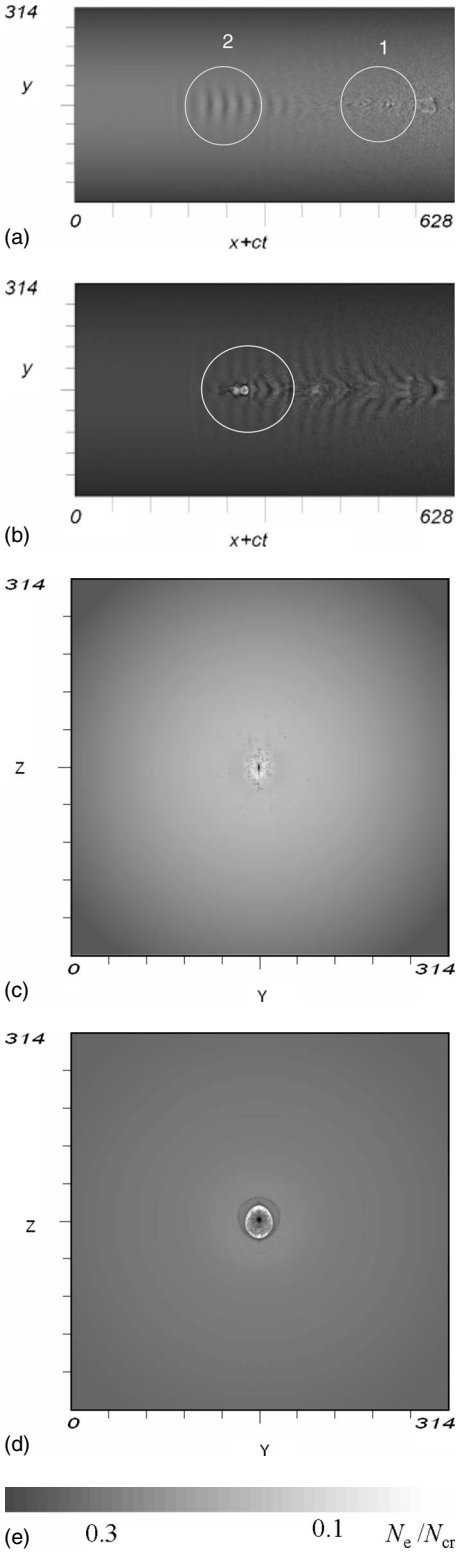

FIG. 9. Snapshots of electron density profiles in the plasma channel $N_{eD}=3\times10^{20}$ cm^{-3} and $\Delta=3$ irradiated by 15-mJ λ^2 (a),(c) and 15-mJ λ^3 (b),(d) laser pulses: (1) vicinity of laser focus and (2) the vicinity of regular wake.

electron spatial distribution. The maximal density at the cavity front approaches a quarter of the critical density; in the cavity, the electron density is almost zero. The size of the beam inside the cavity equals approximately $4w_0$. The en-

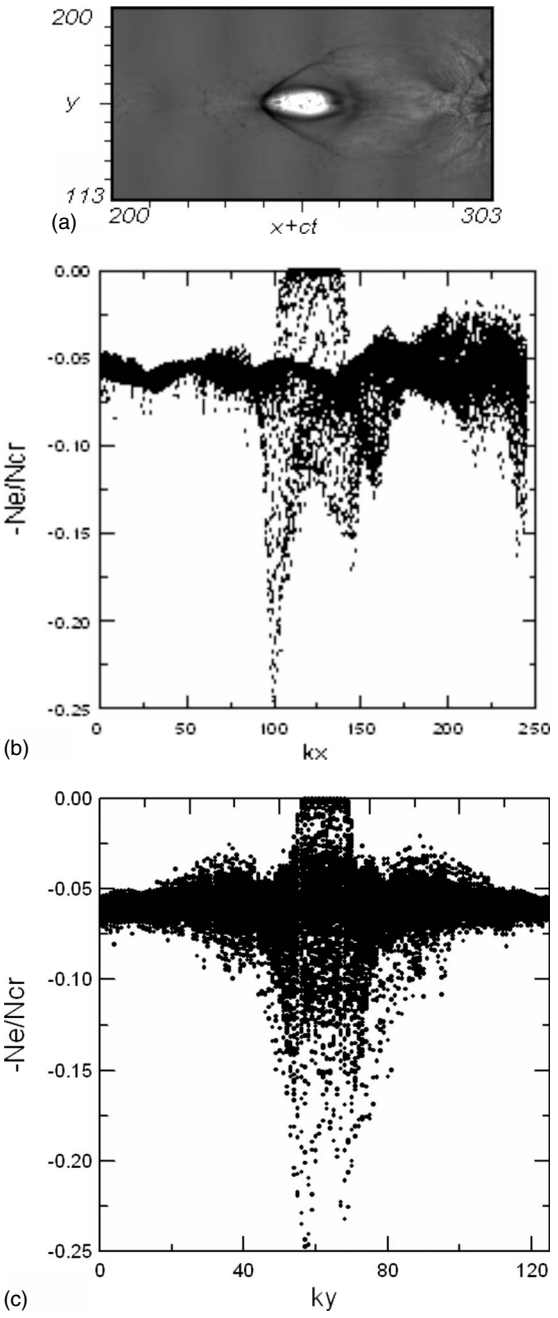

FIG. 10. Magnified image of electron density in the vicinity of the blowout in the plasma channel $N_{eD}=3\times10^{20}$ cm^{-3} and $\Delta=3$ irradiated by a 15-mJ λ^3 laser pulse: (a) in the plane $z=0$ and (b), (c) 1D plots.

ergy distributions in both cases of λ^2 and λ^3 laser pulses are shown in Fig. 11. The distributions are close to a Maxwell-like distribution with an efficient temperature. Such electron beams may generate a high-brightness bremsstrahlung radiation in the MeV range.

III. MODERATE-ENERGY λ^3 LASER PULSES

When the energy of the λ^3 pulse is increased up to 150 mJ, the blowout acceleration regime becomes dominant.

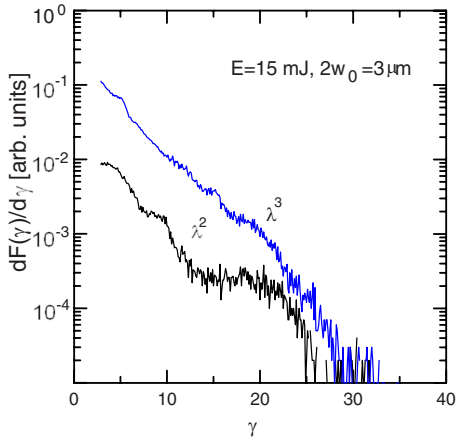

FIG. 11. (Color online) Energy distribution of electrons accelerated by 15-mJ λ^3 and 15-mJ λ^2 laser pulses in the plasma channel $N_{eD}=3\times10^{20}$ and $\Delta=3$.

We make several runs for the λ^3 laser pulse propagation in a channel with different N_{eD} (from 5×10^{19} cm^{-3} up to 3×10^{20} cm^{-3} and $\Delta=3$). In Fig. 12 the dynamics of the laser field is shown in the case of the lowest plasma density. Similar to a low-energy laser pulse, the moderate-energy laser pulse is guided in the plasma channel; the laser field is 30% of the maximal after the pulse passes a 0.42-mm distance. Oscillations of the laser pulse waist, which is typical for the guiding of a laser pulse in the plasma channel, are clearly seen. The electron acceleration length therefore can be quite long for electrons to acquire a high energy. In Fig. 13 the energy distribution of accelerated electrons in this case is presented for different plasma densities. The dependence of the maximal energy is very typical [12]: with the density increase the energy goes down, while the energy range $\varepsilon\sim35-40$ MeV, where accelerated electrons constitute a monoenergetic bunch, does not depend considerably on the plasma density. The total charge of electrons with energy over 10 MeV is 5.4 nC. The electrons constitute a bunch with emittance better than 1π mm mrad and a rather low-energy spread of 35–45 MeV and the total charge of about 1.2 nC. However, the characteristics of the accelerated electrons require special consideration.

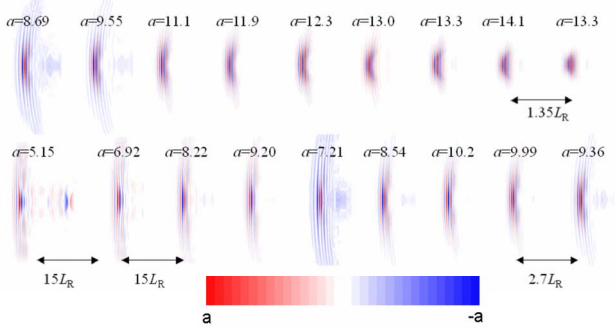

FIG. 12. (Color online) Dynamics of the z component of the electric field of a 150-mJ λ^3 pulse focused in the plasma channel with $N_{eD}=6\times10^{19}$ cm^{-3} and $\Delta=3$. The laser pulse propagates from the right to left; the distance of output and the maximal value of the field, a, are given in the figures.

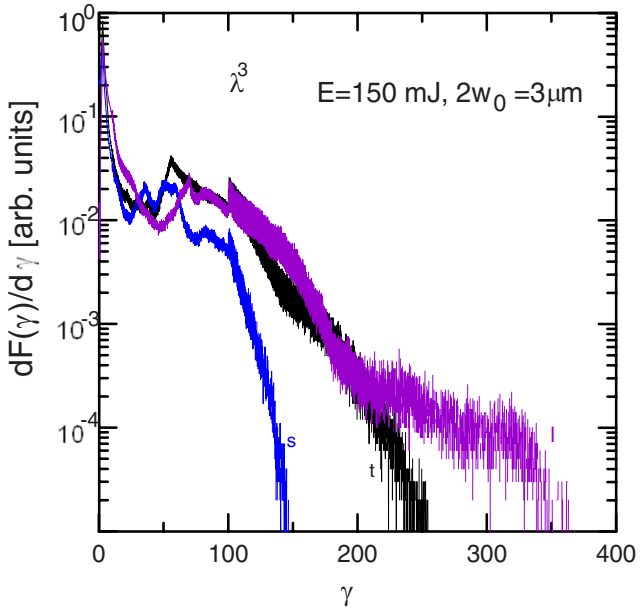

FIG. 13. (Color online) Energy distribution of electrons accelerated by 150-mJ λ^3 laser pulses in the plasma channels $N_{eD}=3\times10^{19}$ (l), $N_{eD}=6\times10^{19}$ (t), $N_{eD}=3\times10^{20}$ (s), and $\Delta=3$.

Similar to a low-energy laser pulse, the moderate-energy laser pulse provokes strong electron self-injection in the vicinity of its focus point. However, the total charge loaded is so high that injected electrons result in the wake dynamics, installing the electron-hose instability and/or wiggling instability.

Quite generally, effects of electron loading can be understood in the framework of an approach used for analysis of the electron-hose instability in the "ion-focus regime" [22–24] of the electron beam propagation. In this approach, the mutual effect of a transverse electron beam displacement δr in a plasma channel and a hose displacement of the channel, δl, is considered in the frozen field approximation. According to Ref. [24], these displacements obey the following equations:

$$\left(\frac{\partial^2}{\partial s^2}+\omega_0^2\right)\delta l(x,t+x/c)-\frac{R_B^2N_B}{R_c^2N_e}\omega_0^2\delta r(x,t+x/c)=0,$$

$$\left(\frac{\partial}{\partial x}\gamma\frac{\partial}{\partial x}+\gamma k_\beta^2\right)\delta r(x,t+x/c)-\frac{\gamma}{\gamma_0}k_\beta^2\delta l(x,t+x/c)=0, \quad (2)$$

where x is the direction of laser pulse propagation, $s=x+t/c$, R_B and R_C are the radii of the beam and the channel, N_B and N_e are the density of the beam and plasma electrons outside the channel (plasma electrons are supposed to be completely evacuated from the channel), γ and γ_0 are the relativistic factors of beam electrons and plasma electrons, and $\omega_0=\omega_{\rm pl}/2^{1/2}$ and $k_\beta\sim\omega_\beta/c$ the betatron wave number, $\omega_\beta=\omega_{\rm pl}/(2\gamma)^{1/2}$. In the case of a laser pulse, we cannot set $\gamma_0=1$ and $N_BR_B^2==N_eR_C^2$.

The dispersion ratio follows from Eq. (2) immediately after substitution of a solution in the form $\exp(ikx+i\omega s)$:

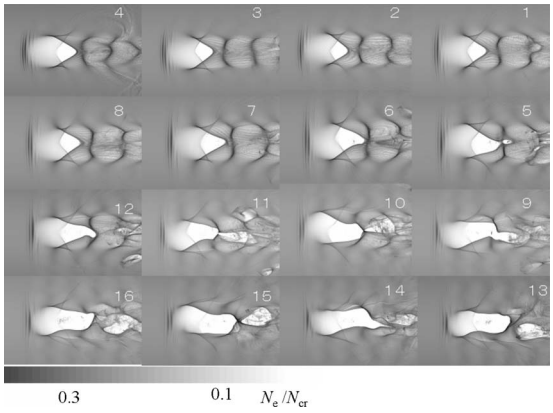

FIG. 14. Evolution of the electron density in the first bucket of the wake of a 150-mJ λ^3 laser pulse in the plasma channel $N_{eD}=6\times10^{19}$ and $\Delta=3$. The snapshots are presented after the $1.5L_R$ distance.

$$k=\pm\sqrt{1-(R_B^2N_B/\gamma_0R_C^2N_e)/[1-\omega^2/\omega_0^2]},$$

with clear growth at ω increasing to ω_0. This instability results both in the beam hosing and in the deformation of the laser wake. However, if relativistic electrons constitute the cavity shell, this instability may be considerably suppressed.

The dynamics of the laser wake in the lower-density channel is shown in Fig. 14. The parameter from the dispersion equation $R_B^2N_B/\gamma_0R_C^2N_e\approx3\times10^{-3}$ is small, and the electron-hose instability develops for a long time. In the beginning, one can observe an oscillation of the cavity rear in the direction of laser polarization at the frequency close to the betatron frequency; an exact calculation of the frequency is difficult in view of the strong nonuniformity of the plasma electron distribution. After the pulse passes approximately 160 μm distance, the oscillation becomes irregular; a portion of electrons constituting the cavity shell are deviated and move at 30°–45° to the laser pulse propagation axis. In Fig. 15 the transverse profile of the electron spatial distribution in the first bucket is presented. The cavity oscillation and the loaded beam modulation are clearly seen. The frequencies of these oscillations are different. The beam frequency is approximately the betatron frequency with $\gamma=65$. To understand this we plot the energy distribution of self-injected electrons in the first bucket. The beam electrons constitute a quite narrow distribution with the maximum around $\gamma_{\max}=70$. The cavity oscillation frequency is higher; this is the influence of lower-energy injected electrons that constitute the rear side of the cavity. An increase of the plasma density results in a stronger electron-hose instability, while the laser pulse hosing is not essential. In Figs. 16(a) and 16(b) the loaded electron hosing in the direction of the laser polarization is seen. In the direction perpendicular to the laser polarization, Fig. 16(c), the beam is quite symmetrical; no hosing is observed. This looks like the laser pulse hosing that usually appears in the direction of the pulse polarization. However, only the electron bunch trajectory bends, while the laser pulse propagates straightforwardly. The fact is that the initial density perturbation necessary for the development of the

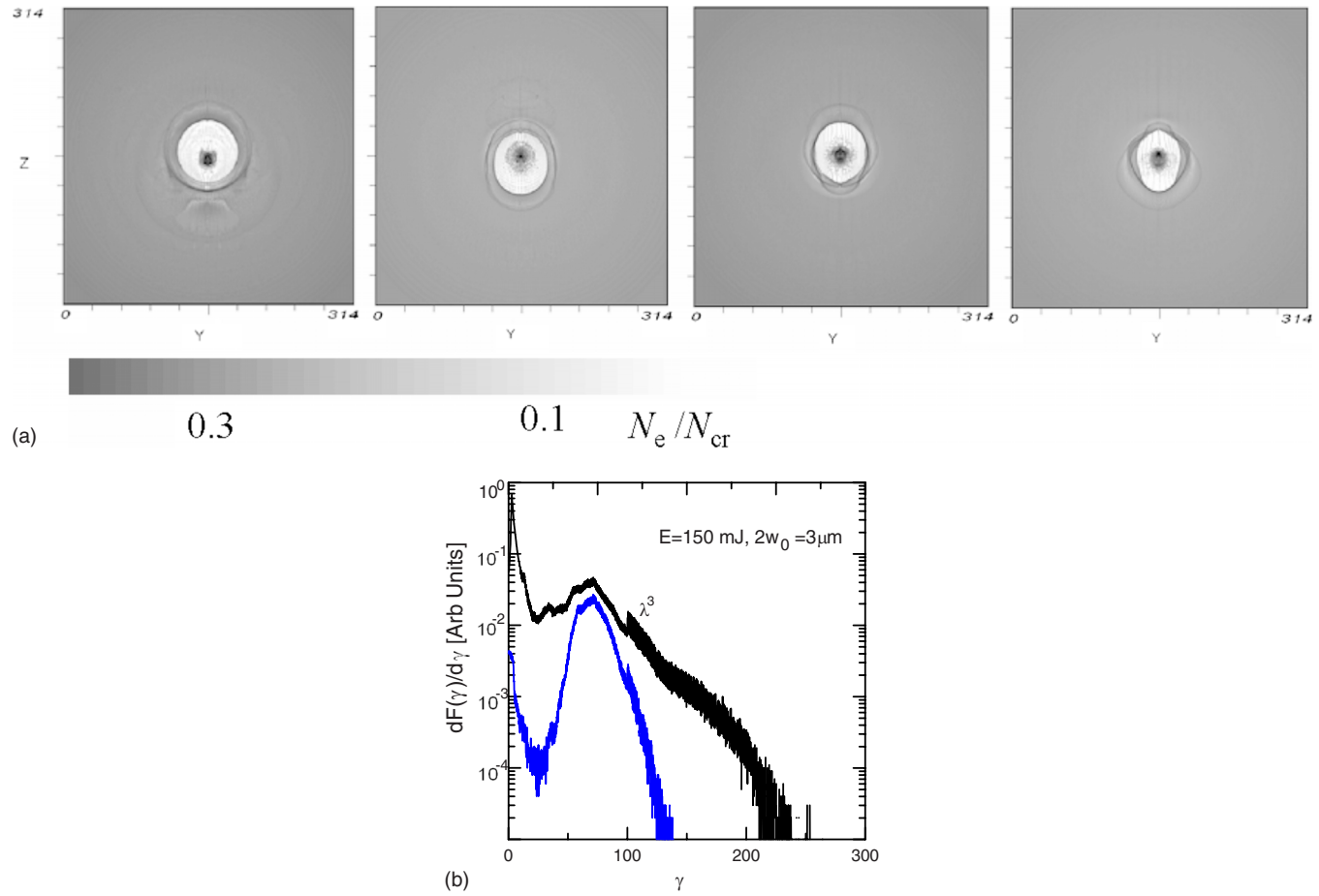

FIG. 15. (Color online) Transverse profile of the electron density in the first bucket as given in Fig. 14(a) and energy distribution of the electron in the first bucket extracted from the total energy distribution (b).

hosing instability is provoked by the laser pulse in the direction of polarization.

IV. 1-J λ^3 LASER PULSE

1-J λ^3 laser pulses can produce strong relativistic plasma: the ponderomotive potential of such a pulse is approximately $mc^2a_0 \sim 20$ MeV at the focus point. We make several runs for such laser pulses in uniform underdense plasma and plasma channels.

The dynamics of a laser pulse focused in a uniform plasma with density $N_e=3\times10^{19}$ cm^{-3} is shown in Fig. 17(a). There is no pulse self-guiding: after reaching the maximal intensity in the focus point, $a_0 \sim 40$, the pulse diffracts. The diffraction is slower that that in vacuum. Nevertheless, after the laser pulse propagates about 100 μm, its intensity becomes of the order of $I=10^{19}$ W/cm^2. A plasma channel with $N_{eD}=9\times10^{19}$ cm^{-3} and $\Delta=3$ does not help much. As shown in Fig. 17(b), the pulse diffraction is almost as fast as that in the uniform plasma; the self-guiding starts at a pulse intensity 100 times as small as the maximal at the focus point.

Despite the rapid diffraction, the interaction of such a high-energy λ^3 laser pulse with underdense plasma is strong. In contrast to the localized electron injection with lower-energy laser pulses, the electron self-injection with a 1-J pulse appears not only in the vicinity of focus: the pulse intensity is strong enough for continuous electron self-injection in a distance of $\sim 10L_R$. This results in the generation of a long modulated electron beam. The dynamics of formation of such a beam in uniform plasma is shown in Fig. 18(a) in the two cross sections: parallel and perpendicular to the laser polarization. One can see that the beam modulation is a result of the multiple self-injection [11] rather than a betatron modulation of the beam.

However, the betatron oscillation plays an important role. The cavity is modulated with the laser frequency in this case. This modulation exerts a beam oscillation that results in beam radiation. Magnified images of the beam and its field are given in Fig. 18(b). Approximately 15 bunches are seen in the beam; the bunch length is approximately $\lambda/2$, where λ is the laser pulse wavelength. A well-structured radiation field is also seen in the figure. (However, the spatial resolution of the PIC simulation, $\Delta x \sim \lambda/20$, is not enough for a complete characterization of the beam radiation.) An important fact is that the cavity is modulated in this case not only with the betatron frequency $\omega_{pl}/\gamma^{1/2}$ [22], but also with the laser pulse frequency $\omega=2\pi c/\lambda$. This modulation appears in the direction of the laser pulse polarization and is asymmetric. Bunches of injected electrons also appear repeatedly with a period close to the laser wavelength. Due to the cavity

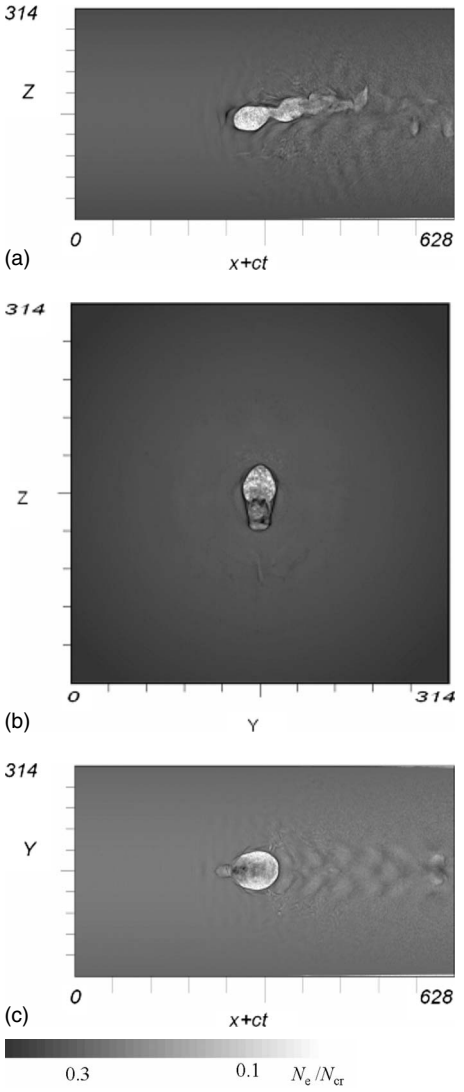

FIG. 16. Snapshots of electron density profiles in the plasma channel $N_{eD}=3\times10^{20}$ cm^{-3} and $\Delta=3$ irradiated by a 150-mJ λ^3 laser pulse after the laser pulse passed $10L_R$ after the focus position. An arrow in the transverse profile (b) shows the position of the electron beam center.

modulation, bunches radiate, and, therefore, the cavity is a "moving ondulator" or a "moving wiggler:" all bunches radiate at the same positions in the reference frame moving with the cavity, while in the laboratory reference frame these positions are shifted. A period of the radiation is $T=(T_{\rm inj}v_{\rm gr}+T_{\rm acc}v_e)/2\pi c$, where $T_{\rm inj}$ and $T_{\rm acc}$ are the period of the multiple self-injection and the acceleration time, and $v_{\rm gr}$ and v_e are the group velocity of the laser pulse and the velocity of accelerated electrons in a bunch. The K number determining the type of radiation [25] is in this case approximately $K\sim\gamma\delta l/R_C$, where δl is the modulation amplitude, R_C is the cavity radius, and γ is the electron relativistic factor. For the current calculation K equals 0.3: the ondulator case. Spatially coherent x-ray radiation at the fundamental frequency $\omega_{\rm rad}=2\pi c\gamma^2/[T(1+K^2+\gamma^2\theta^2)]$ corresponding to the energy 0.7–0.8 keV ($\theta=0$) is expected.

The use of a plasma channel $N_{eD}=9\times10^{19}$ cm^{-3} and $\Delta=3$ may improve the quality of the moving ondulator. The

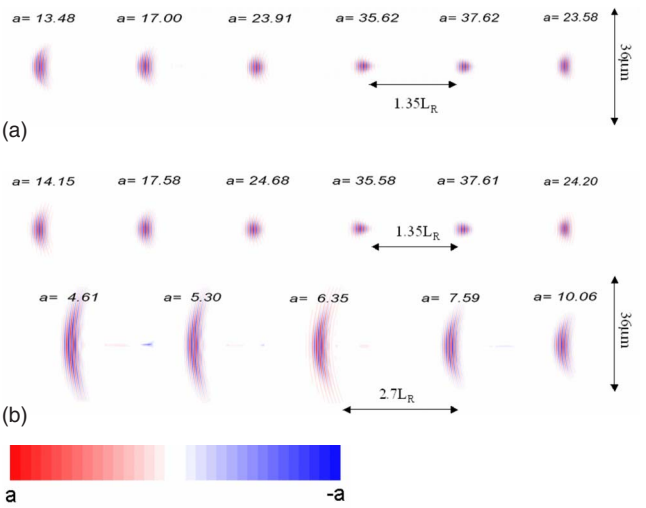

FIG. 17. (Color online) Dynamics of the z component of the electric field of a 1-J λ^3 pulse focused in a uniform plasma $N_{e0}=3\times10^{20}$ cm^{-3} (a) and the plasma channel with $N_{eD}=6\times10^{19}$ cm^{-3} and $\Delta=3$ (b). The laser pulse propagates from the right to left; the distance of output and the maximal value of the field, a, are given in the figures.

dynamics of injected electrons in this case is shown in Fig. 19. The scenario of beam formation is very similar to that in uniform plasma. The presence of a plasma channel does not result much in high-intensity laser pulse evolution. However, the number of bunches considerably increases, up to 32, due to the better guiding of the pulse in the channel. The K num-

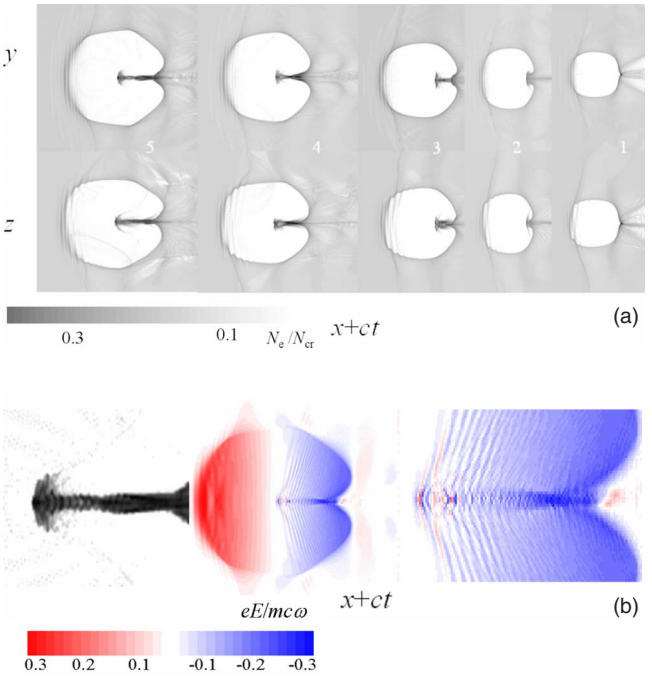

FIG. 18. (Color online) Evolution of the electron density in the first bucket of the wake of a 1-J λ^3 laser pulse in a uniform plasma: $N_{eD}=3\times10^{19}$ and $\Delta=3$ (a) (the snapshots are presented after the $1.5L_R$ distance) and magnified images of the electron beam and its field (b) for snapshot N5.

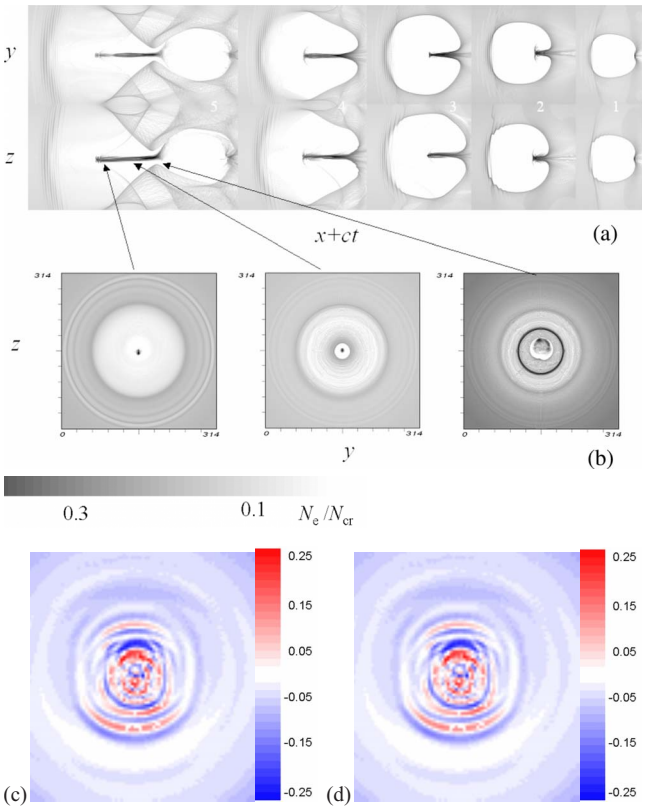

FIG. 19. (Color online) Evolution of the electron density in the first bucket of the wake of a 1-J λ^3 laser pulse in the plasma channel $N_{eD}=6\times10^{19}$ and $\Delta=3$ (a) (the snapshots are presented after the $1.5L_R$ distance) and transverse profiles of the electron density in the first bucket (b) and the beam field (d) for snapshot N5.

ber also becomes smaller, approximately 0.1. In Fig. 19(b) the transverse bunch displacement from the axis is clearly seen. The beam length is limited by the breaking of the first bucket of the wake. The transverse structure of the beam radiation is also shown. The maximal intensity of beam radiation increases with time faster than the beam length, which may be a sign of ondulator radiation. However, a quantitative study requires a much better spatial resolution of PIC simulation.

The electron energy distributions for these cases are shown in Fig. 20. Surprisingly, the maximal energy of accelerated electrons is small: 34 MeV in uniform plasma and 25 MeV in the plasma channel. In the plasma channel, a quite monoenergetic beam is observed with energy equal to approximately 20 MeV. The total charge of monoenergetic particles is high, over 4.3 nC

V. CONCLUSION

In conclusion, we have studied the electron self-injection and acceleration by wakes of tightly focused λ^3 (and λ^2)

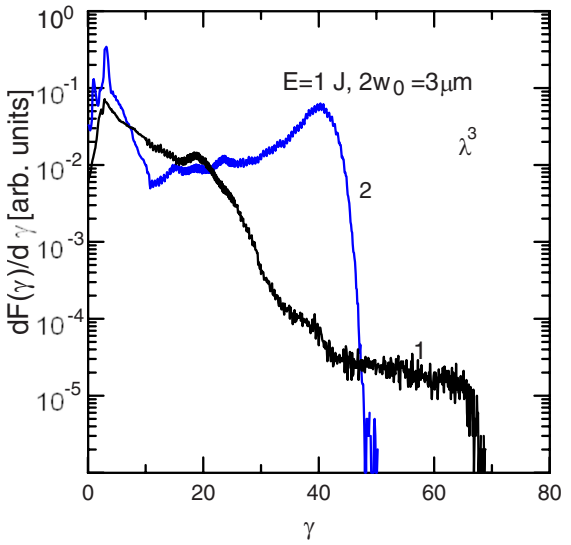

FIG. 20. (Color online) Energy distribution of electrons accelerated by 1-J λ^3 laser pulses in a uniform plasma (1) and the plasma channel $N_{eD}=6\times10^{19}$ and $\Delta=3$ (2).

laser pulses in underdense plasma by means of fully relativistic, real-geometry particle-in-cell simulation. We have found efficient electron self-injection in the vicinity of the laser focus with the consequent strong blowout regime of electron acceleration that is different from known acceleration regimes. This acceleration mechanism can provide high-charge multi-MeV electron bunches at low energy of the laser pulses: approximately 50 nC per 1-J of the laser pulse energy; the charge of the bunch with a low emittance of $\ll1\pi$ mm mrad exceeds 10 nC/J. Such bunches can be a source of ultimately bright bremsstrahlung radiation in the multi-MeV energy range. However, we have also observed electron-hose and wiggling instabilities during electron acceleration by the laser wake field. Such instabilities appear with a moderate energy laser pulse propagating in plasma channels; the mechanism of electron-hose instability is relative to that which appears in the plasma wake field accelerators.

1-J level λ^3-laser pulses cannot self-guide in underdense plasma and plasma channels. However, despite strong diffraction, the interaction of such a laser pulse with plasma is very efficient, resulting in the generation of a tens of MeV, quasimonoenergetic electron beam with subfemtosecond modulation. This allows realization of the concept of a moving ondulator or moving wiggler with production coherent x rays in the 1-keV range.

Although presently λ^3 laser pulses have only a few-mJ energy, we anticipate that the development of high-energy λ^3 laser systems may open the way for the creation of coherent, jitter-free hard x-ray sources.

[1] S. P. D. Mangles, D. Murphy, Z. Najmudin, A. G. R. Thomas, J. L. Collier, A. B. Dangor, E. J. Divall, P. S. Foster, J. G. Gallacher, C. J. Hooker, D. A. Jaroszyanski, A. J. Langley, W. B. Mori, P. A. Norreys, F. S. Tsung, R. Viskop, B. R. Walton, and K. Krushelnick, Nature (London) **431**, 535 (2004); C. G. R. Geddes, Cs. Toth, J. van Tilborg, E. Esarey, C. B. Schroeder, D. L. Bruhwiler, C. Nieter, J. R. Cary, and W. P. Leemans, *ibid.* **431**, 538 (2004); J. Faure, Y. Glinec, A. Pukhov, S. Kiselev, S. Gordienko, E. Lefebvre, J. P. Rousseau, F. Burgy, and V. Malka, *ibid.* **431**, 541 (2004); K. Koyama, E. Miura, S. Kato, N. Saito, S. Masuda, and M. Adachi, J. Part. Accel. Soc. Jpn. **1**, 158 (2004); A. Yamazaki, H. Kotaki, and I. Daito, Phys. Plasmas **12**, 093101 (2005); W. P. Leemans, B. Nagler, S. M. Hooker *et al.*, Nat. Phys. **2**, 696 (2006).

[2] T. Hosokai, K. Kinoshita, A. Zhidkov, A. Maekawa, A. Yamazaki, and M. Uesaka, Phys. Rev. Lett. **97**, 075004 (2006); Phys. Rev. E **73**, 036407 (2006); Phys. Plasmas **11**, L57 (2004); Phys. Rev. E **67**, 036407 (2003).

[3] G. Mourou, Z. Chang, A. Maksimchuk, J. Nees, S. V. Bulanov, V. Yu. Bychenkov, T. Zh. Esirkepov, N. M. Naumova, F. Pegoraro, and H. Ruhl, Plasma Phys. Rep. **28**, 14 (2002).

[4] G. A. Mourou, T. Tajima, and S. V. Bulanov, Rev. Mod. Phys. **78**, 309 (2006).

[5] N. M. Naumova, J. A. Nees, I. V. Sokolov, B. Hou, and G. A. Mourou, Phys. Rev. Lett. **92**, 063902 (2004).

[6] S. Bulanov, N. Naumova, F. Pegoraro, and J. Sakai, Phys. Rev. E **58**, R5257 (1998); T. Y. Chien, C. L. Chang, C. H. Lee, J. Y. Lin, J. Wang, and S. Y. Chen, Phys. Rev. Lett. **94**, 115003 (2005).

[7] S. V. Bulanov, F. Pegoraro, A. M. Pukhov, and A. S. Sakharov, Phys. Rev. Lett. **78**, 4205 (1997).

[8] N. Naumova, J. Koga, K. Nakajima *et al.*, Phys. Plasmas **8**, 4149 (2001).

[9] A. Zhidkov, J. Koga, T. Hosokai *et al.*, Phys. Plasmas **11**, 5379 (2004).

[10] T. Ohkubo, A. Zhidkov, T. Hosokai *et al.*, Phys. Plasmas **13**, 033110 (2006).

[11] A. Oguchi, A. Zhidkov, K. Takano, E. Hotta, K. Nemoto, and K. Nakajima, Phys. Plasmas **15**, 043102 (2008).

[12] E. Eseray, P. Sprangle, and A. Ting, IEEE Trans. Plasma Sci. **24**, 252 (1996).

[13] M. Born and E. Wolf, *Principles of Optics* (Cambridge University Press, Cambridge, England, 1980), p. 435.

[14] S. Sepke and D. Umstadter, Opt. Lett. **31**, 1447 (2006).

[15] 15 and 150 mJ are the maximal pulse energies, nowadays, in 10- and 1-kHz laser systems: I. Matsushima, H. Yashiro, and T. Tomie, Opt. Lett. **31**, 2066 (2006); Jpn. J. Appl. Phys., Part 2 **44**, L823 (2005).

[16] T. Hosokai, K. Kinoshita, T. Ohkubo *et al.*, Phys. Rev. E **73**, 036407 (2006).

[17] A. Ting, E. Esarey, and P. Sprangle, Phys. Fluids B **2**, 1390 (1990).

[18] A. Zhidkov, K. Nemoto, T. Nayuki, Y. Oishi, and T. Fuji, Phys. Rev. E **76**, 016401 (2007) and reference therein.

[19] T. Ohkubo, S. V. Bulanov, A. Zhidkov, T. Esirkepov, J. Koga, M. Uesaka, and T. Tajima, Phys. Plasmas **13**, 103101 (2006).

[20] T. Hosokai, A. Zhidkov, A. Yamazaki *et al.* (unpublished).

[21] G. Bonnaud, H. S. Brandi, C. Manus *et al.*, Phys. Plasmas **1** 968 (1994); H. S. Brandi, C. Manus, G. Mainfray, and T. Lehner, Phys. Fluids B **5**, 3539 (1993); Phys. Rev. E **47**, 3780 (1993); Phys. Fluids B **5**, 3539 (1993).

[22] C. Huang, W. Lu, M. Zhou *et al.*, Phys. Rev. Lett. **99**, 255001 (2007).

[23] M. Lampe, G. Joyce, and S. P. Slinker, Phys. Fluids B **5**, 1888 (1993).

[24] D. H. Whittum, W. M. Sharp, S. S. Yu, M. Lampe, and G. Joyce, Phys. Rev. Lett. **67**, 991 (1991); A. A. Geraci and D. H. Whittum, Phys. Plasmas **7**, 3431 (2000).

[25] J. D. Jackson, *Classical Electrodynamcis*, 3rd ed. (Wiley, New York, 1998).